Chapter 2

Numerical Tests

We here collect a few numerical tests, in order to put into evidence the potentialities of HBVMs [4, 6, 7].

Test problem 1

Let us consider the problem characterized by the polynomial Hamiltonian (4.1) in [19],

$$H(p,q) = \frac{p^3}{3} - \frac{p}{2} + \frac{q^6}{30} + \frac{q^4}{4} - \frac{q^3}{3} + \frac{1}{6}, \tag{2.1}$$

having degree $\nu = 6$, starting at the initial point $y_0 \equiv (q(0), p(0))^T = (0, 1)^T$, so that $H(y_0) = 0$. For such a problem, in [19] it has been experienced a numerical drift in the discrete Hamiltonian, when using the fourth-order Lobatto IIIA method with stepsize $h = 0.16$, as confirmed by the plot in Figure 2.1. When using the fourth-order Gauss-Legendre method the drift disappears, even though the Hamiltonian is not exactly preserved along the discrete solution, as is confirmed by the plot in Figure 2.2. On the other hand, by using the fourth-order HBVM(6,2) with the same stepsize, the Hamiltonian turns out to be preserved up to machine precision, as shown in Figure 2.3, since such method exactly preserves polynomial Hamiltonians of degree up to 6. In such a case, according to the last item in Remark 7, the numerical solutions obtained by using the Lobatto nodes $\{c_0 = 0, c_1, \ldots, c_6 = 1\}$ or the Gauss-Legendre nodes $\{c_1, \ldots, c_6\}$ are the same. The fourth-order convergence of the method is numerically verified by the results listed in Table 2.1.

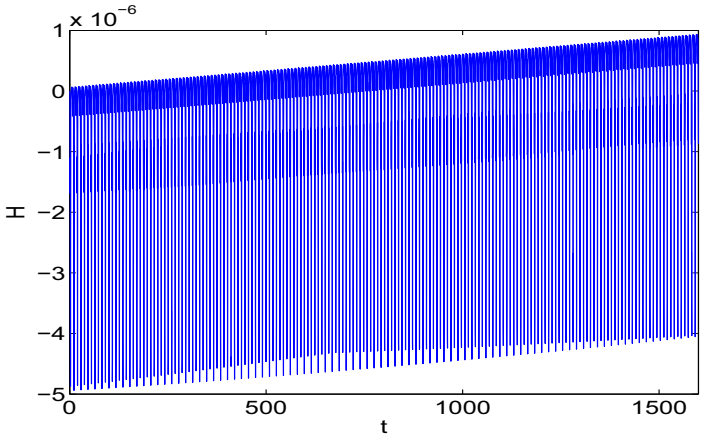

Figure 2.1: Fourth-order Lobatto IIIA method, $h = 0.16$, problem (2.1): drift in the Hamiltonian.

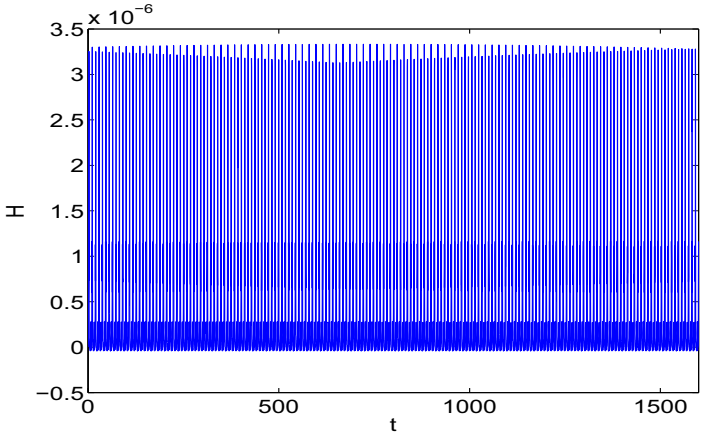

Figure 2.2: Fourth-order Gauss-Legendre method, $h = 0.16$, problem (2.1): $H \approx 10^{-6}$.

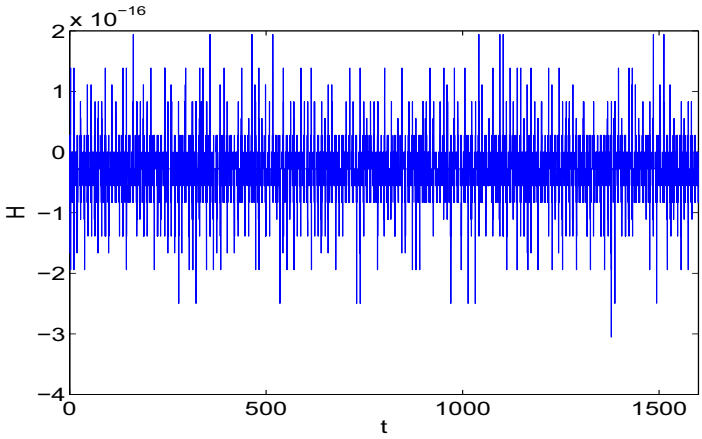

Figure 2.3: Fourth-order HBVM(6,2) method, $h = 0.16$, problem (2.1): $H \approx 10^{-16}$.

Test problem 2

The second test problem, having a highly oscillating solution, is the Fermi-Pasta-Ulam problem (see [20, Section I.5.1]), modelling a chain of $2m$ mass points connected with alternating soft nonlinear and stiff linear springs, and fixed at the end points. The variables $q_1, ..., q_{2m}$ stand for the displacements of the mass points, and $p_i = \dot{q}_i$ for their velocities. The corresponding Hamiltonian, representing the total energy, is

$$H(p,q) = \frac{1}{2}\sum_{i=1}^{m}\left(p_{2i-1}^2 + p_{2i}^2\right) + \frac{\omega^2}{4}\sum_{i=1}^{m}\left(q_{2i} - q_{2i-1}\right)^2 + \sum_{i=0}^{m}\left(q_{2i+1} - q_{2i}\right)^4, \quad (2.2)$$

with $q_0 = q_{2m+1} = 0$. In our simulation we have used the following values: $m = 3$, $\omega = 50$, and starting vector

$$p_i = 0, \quad q_i = (i-1)/10, \qquad i = 1, \ldots, 6.$$

In such a case, the Hamiltonian function is a polynomial of degree 4, so that the fourth-order HBVM(4,2) method, either when using the Lobatto nodes or the Gauss-Legendre nodes, is able to exactly preserve the Hamiltonian, as confirmed by the plot in Figure 2.6, obtained with stepsize $h = 0.05$. Conversely, by using the same stepsize, both the fourth-order Lobatto IIIA and Gauss-Legendre methods provide only an approximate conservation of the Hamiltonian, as shown in the plots in Figures 2.4 and 2.5, respectively. The fourth-order convergence of the HBVM(4,2) method is numerically verified by the results listed in Table 2.2.

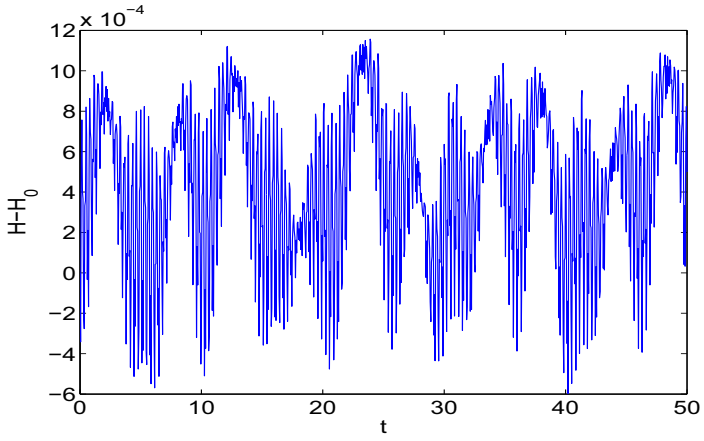

Figure 2.4: Fourth-order Lobatto IIIA method, $h = 0.05$, problem (2.2): $|H - H_0| \approx 10^{-3}$.

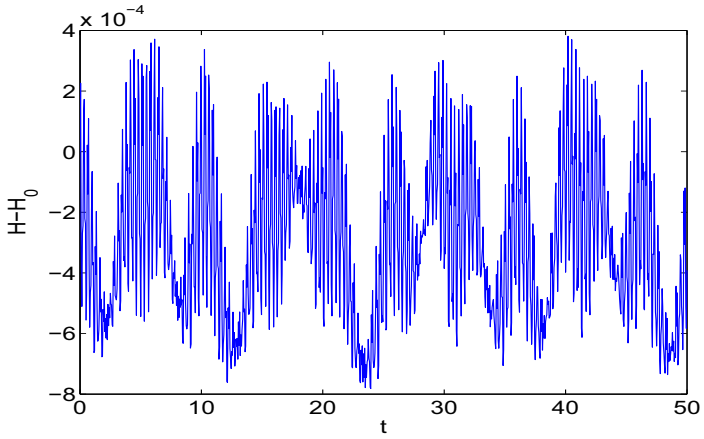

Figure 2.5: Fourth-order Gauss-Legendre method, $h = 0.05$, problem (2.2): $|H - H_0| \approx 10^{-3}$.

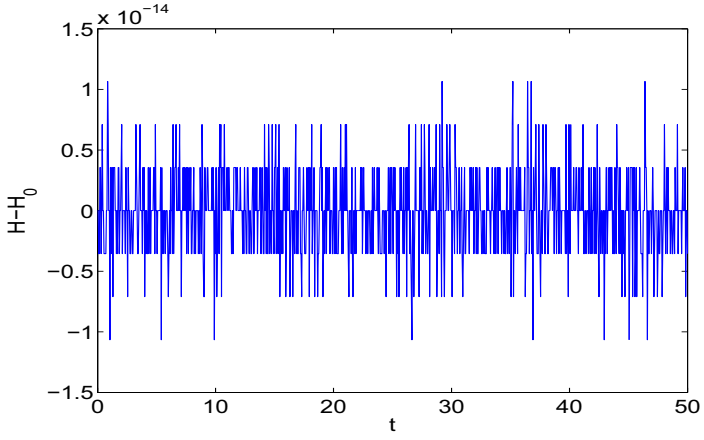

Figure 2.6: Fourth-order HBVM(4,2) method, $h = 0.05$, problem (2.2): $|H - H_0| \approx 10^{-14}$.

Test problem 3 (non-polynomial Hamiltonian)

In the previous examples, the Hamiltonian function was a polynomial. Nevertheless, as observed above, also in this case HBVM(k,s) are expected to produce a *practical* conservation of the energy when applied to systems defined by a non-polynomial Hamiltonian function that can be locally well approximated by a polynomial. As an example, we consider the motion of a charged particle in a magnetic field with Biot-Savart potential.[1] It is defined by the Hamiltonian [6]

$$H(x,y,z,\dot{x},\dot{y},\dot{z}) = \frac{1}{2m}\left[\left(\dot{x}-\alpha\frac{x}{\varrho^2}\right)^2+\left(\dot{y}-\alpha\frac{y}{\varrho^2}\right)^2+(\dot{z}+\alpha\log(\varrho))^2\right], \tag{2.3}$$

with $\varrho=\sqrt{x^2+y^2}$, $\alpha = e\,B_0$, m is the particle mass, e is its charge, and B_0 is the magnetic field intensity. We have used the values

$$m=1, \qquad e=-1, \qquad B_0=1,$$

with starting point

$$x=0.5, \quad y=10, \quad z=0, \quad \dot{x}=-0.1, \quad \dot{y}=-0.3, \quad \dot{z}=0.$$

By using the fourth-order Lobatto IIIA method, with stepsize $h=0.1$, a drift is again experienced in the numerical solution, as is shown in Figure 2.7. By using the fourth-order Gauss-Legendre method with the same stepsize, the drift disappears even though, as shown in Figure 2.8, the value of the Hamiltonian is preserved within an error of the order of 10^{-3}. On the other hand, when using the HBVM(6,2) method with the same stepsize, the error in the Hamiltonian decreases to an order of 10^{-15} (see Figure 2.9), thus giving a practical conservation. Finally, in Table 2.4 we list the maximum absolute difference between the numerical solutions over 10^3 integration steps, computed by the HBVM$(k,2)$ methods based on Lobatto abscissae and on Gauss-Legendre abscissae, as k grows, with stepsize $h=0.1$. We observe that the difference tends to 0, as k increases. Finally, also in this case, one verifies a fourth-order convergence, as the results listed in Table 2.3 show.

[1] This kind of motion causes the well known phenomenon of *aurora borealis*.

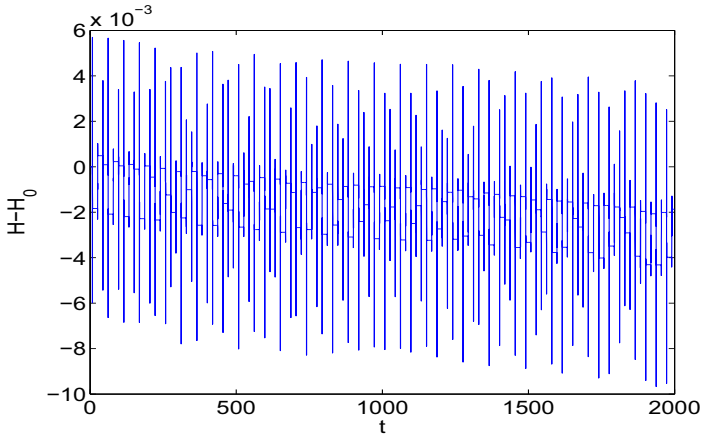

Figure 2.7: Fourth-order Lobatto IIIA method, $h = 0.1$, problem (2.3): drift in the Hamiltonian.

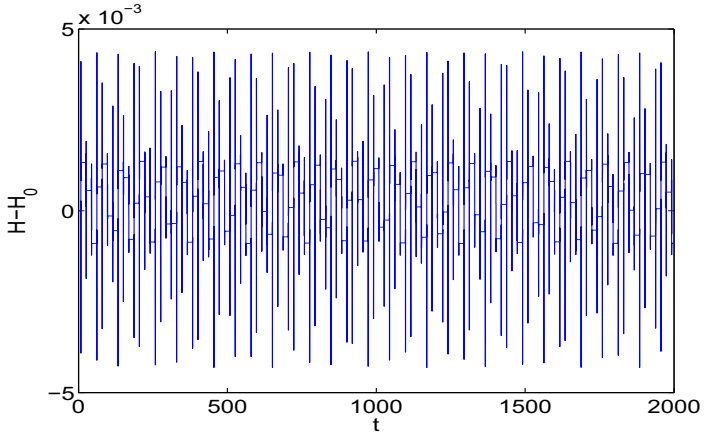

Figure 2.8: Fourth-order Gauss-Legendre method, $h = 0.1$, problem (2.3): $|H - H_0| \approx 10^{-3}$.

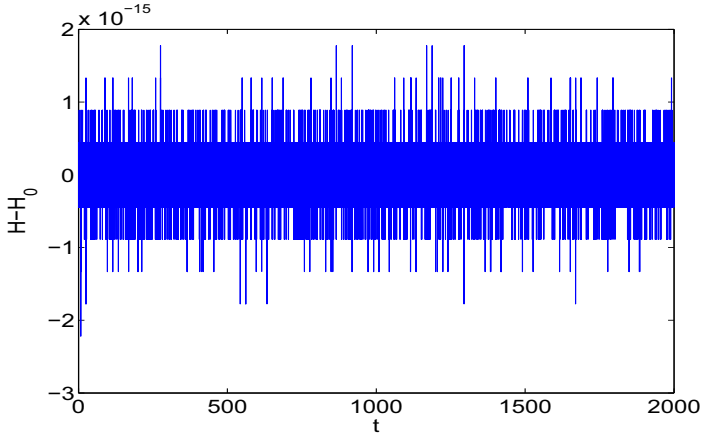

Figure 2.9: Fourth-order HBVM(6,2) method, $h = 0.1$, problem (2.3): $|H - H_0| \approx 10^{-15}$.

Table 2.1: Numerical order of convergence for the HBVM(6,2) method, problem (2.1).

h	0.32	0.16	0.08	0.04	0.02
error	$2.288 \cdot 10^{-2}$	$1.487 \cdot 10^{-3}$	$9.398 \cdot 10^{-5}$	$5.890 \cdot 10^{-6}$	$3.684 \cdot 10^{-7}$
order	–	3.94	3.98	4.00	4.00

Table 2.2: Numerical order of convergence for the HBVM(4,2) method, problem (2.2).

h	$1.6 \cdot 10^{-2}$	$8 \cdot 10^{-3}$	$4 \cdot 10^{-3}$	$2 \cdot 10^{-3}$	10^{-3}
error	3.030	$1.967 \cdot 10^{-1}$	$1.240 \cdot 10^{-2}$	$7.761 \cdot 10^{-4}$	$4.853 \cdot 10^{-5}$
order	–	3.97	3.99	4.00	4.00

Table 2.3: Numerical order of convergence for the HBVM(6,2) method, problem (2.3).

h	$3.2 \cdot 10^{-2}$	$1.6 \cdot 10^{-2}$	$8 \cdot 10^{-3}$	$4 \cdot 10^{-3}$	$2 \cdot 10^{-3}$
error	$3.944 \cdot 10^{-6}$	$2.635 \cdot 10^{-7}$	$1.729 \cdot 10^{-8}$	$1.094 \cdot 10^{-9}$	$6.838 \cdot 10^{-11}$
order	–	3.90	3.93	3.98	4.00

Table 2.4: Maximum difference between the numerical solutions obtained through the fourth-order HBVM$(k, 2)$ methods based on Lobatto abscissae and Gauss-Legendre abscissae for increasing values of k, problem (2.3), 10^3 steps with step-size $h = 0.1$.

k	$h = 0.1$
2	$3.97 \cdot 10^{-1}$
4	$2.29 \cdot 10^{-3}$
6	$2.01 \cdot 10^{-8}$
8	$1.37 \cdot 10^{-11}$
10	$5.88 \cdot 10^{-13}$

Test problem 4 (Sitnikov problem)

The main problem in Celestial Mechanics is the so called N-body problem, i.e. to describe the motion of N point particles of positive mass moving under Newton's law of gravitation when we know their positions and velocities at a given time. This problem is described by the Hamiltonian function:

$$H(\boldsymbol{q},\boldsymbol{p}) = \frac{1}{2}\sum_{i=1}^{N}\frac{||p_i||_2^2}{m_i} - G\sum_{i=1}^{N} m_i \sum_{j=1}^{i-1}\frac{m_j}{||q_i - q_j||_2}, \tag{2.4}$$

where q_i is the position of the ith particle, with mass m_i, and p_i is its momentum.

The Sitnikov problem is a particular configuration of the 3-body dynamics (see, e.g., [30]). In this problem two bodies of equal mass (primaries) revolve about their center of mass, here assumed at the origin, in elliptic orbits in the xy-plane. A third, and much smaller body (planetoid), is placed on the z-axis with initial velocity parallel to this axis as well.

The third body is small enough that the two body dynamics of the primaries is not destroyed. Then, the motion of the third body will be restricted to the z-axis and oscillating around the origin but not necessarily periodic. In fact this problem has been shown to exhibit a chaotic behavior when the eccentricity of the orbits of the primaries exceeds a critical value that, for the data set we have used, is $\bar{e} \simeq 0.725$ (see Figure 2.10).

We have solved the problem defined by the Hamiltonian function (2.4) by the Gauss method of order 4 (i.e., HBVM(2,2) at 2 Gaussian nodes) and by HBVM(18,2) at 18 Gaussian nodes (order 4, 2 fundamental and 16 silent stages), with the following set of parameters in (2.4):

N	G	m_1	m_2	m_3	e	d	h	t_{max}
3	1	1	1	10^{-5}	0.75	5	0.5	1500

where e is the eccentricity, d is the distance of the apocentres of the primaries (points at which the two bodies are the furthest), h is the used time-step, and $[0,\, t_{\text{max}}]$ is the time integration interval. The eccentricity e and the distance d may be used to define the initial condition $[\boldsymbol{q}_0, \boldsymbol{p}_0]$ (see [30] for the details):

$$\begin{aligned}\boldsymbol{q}_0 &= [-\tfrac{5}{2},\ 0,\ 0,\ \tfrac{5}{2},\ 0,\ 0,\ 0,\ 0,\ 10^{-9}]^T,\\ \boldsymbol{p}_0 &= [0,\ -\tfrac{1}{20}\sqrt{10},\ 0,\ 0,\ \tfrac{1}{20}\sqrt{10},\ 0,\ 0,\ 0,\ \tfrac{1}{2}]^T.\end{aligned}$$

First of all, we consider the two pictures in Figure 2.11 reporting the relative errors in the Hamiltonian function and in the angular momentum evaluated along the numerical solutions computed by the two methods. We know that the

HBVM(18,2) precisely conserves Hamiltonian polynomial functions of degree at most 18. This accuracy is high enough to guarantee that the nonlinear Hamiltonian function (2.4) is as well conserved up to the machine precision (see the upper picture): from a geometrical point of view this means that a local approximation of the level curves of (2.4) by a polynomial of degree 18 leads to a negligible error. The Gauss method exhibits a certain error in the Hamiltonian function while, being this formula symplectic, it precisely conserves the angular momentum, as is confirmed by looking at the down picture of Figure 2.11. The error in the numerical angular momentum associated with the HBVM(18,2) undergoes some bounded periodic-like oscillations.

Figures 2.12 and 2.13 show the numerical solution computed by the Gauss method and HBVM(18,2), respectively. Since the methods leave the xy-plane invariant for the motion of the primaries and the z-axis invariant for the motion of the planetoid, we have just reported the motion of the primaries in the xy-phase plane (upper pictures) and the space-time diagram of the planetoid (down picture).

We observe that, for the Gauss method, the orbits of the primaries are irregular in character so that the third body, after performing some oscillations around the origin, will eventually escape the system (see the down picture of Figure 2.12). On the contrary (see the upper picture of Figure 2.13), the HBVM(18,2) method generates a quite regular phase portrait. Due to the large stepsize h used, a sham rotation of the xy-plane appears which, however, does not destroy the global symmetry of the dynamics, as testified by the bounded oscillations of the planetoid (down picture of Figure 2.13) which look very similar to the reference ones in Figure 2.10. This aspect is also confirmed by the pictures in Figure 2.14 displaying the distance of the primaries as a function of the time. We see that the distance of the apocentres (corresponding to the maxima in the plots), as the two bodies wheel around the origin, are preserved by the HBVM(18,2) (down picture) while the same is not true for the Gauss method (upper picture).

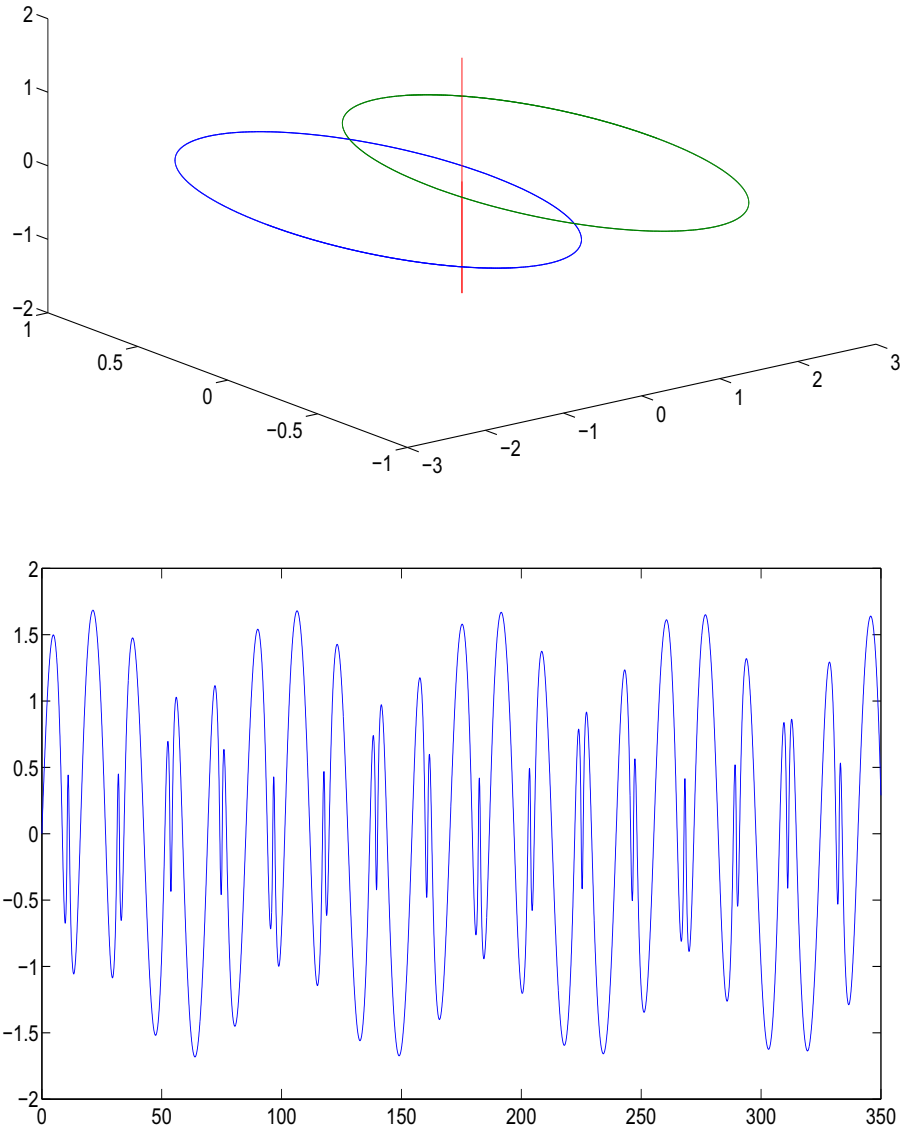

Figure 2.10: The upper picture displays the configuration of 3-bodies in the Sitnikov problem. To an eccentricity of the orbits of the primaries $e = 0.75$, there correspond bounded chaotic oscillations of the planetoid as is argued by looking at the space-time diagram in the down picture.

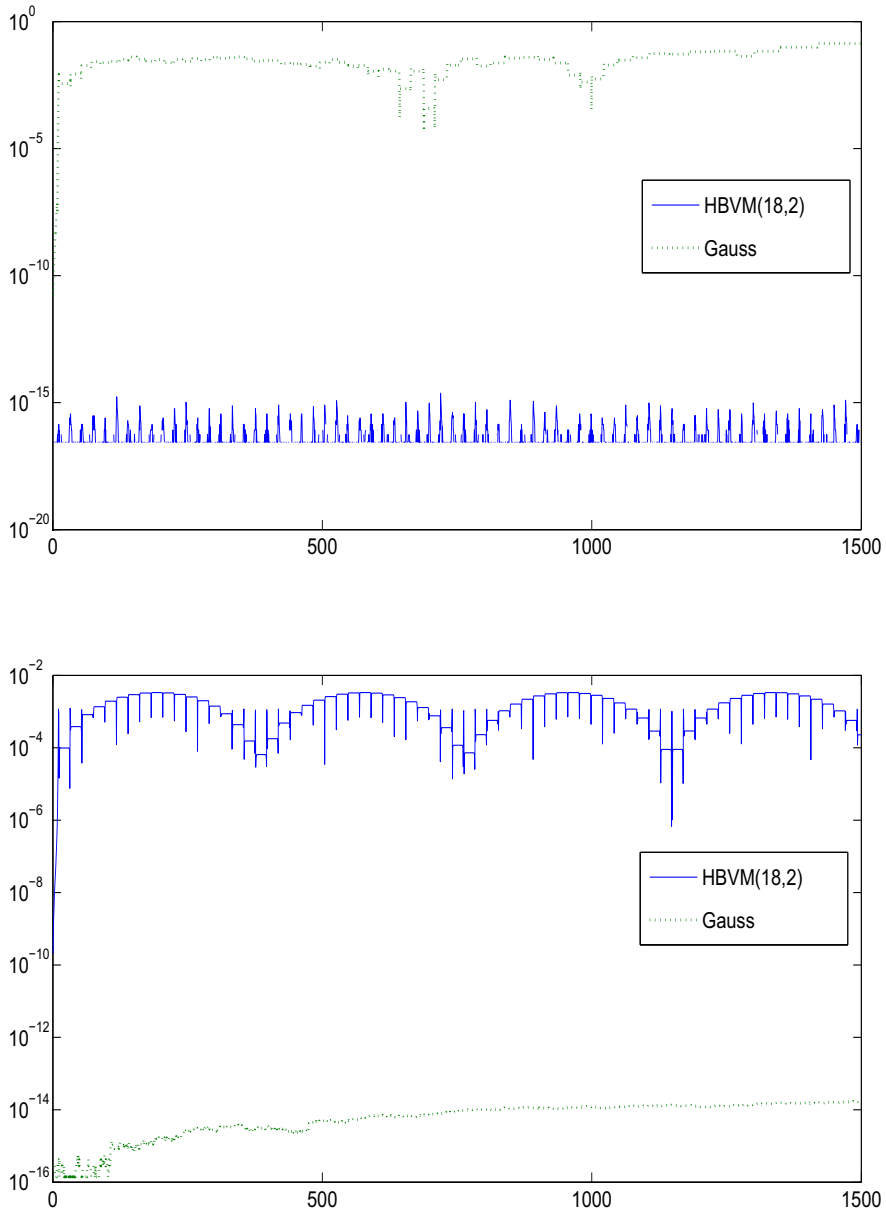

Figure 2.11: Upper picture: relative error $|H(y_n) - H(y_0)|/|H(y_0)|$ of the Hamiltonian function evaluated along the numerical solution of the HBVM(18,2) and the Gauss method. Down picture: relative error $|M(y_n) - M(y_0)|/|M(y_0)|$ of the angular momentum evaluated along the numerical solution of the HBVM(18,2) and the Gauss method.

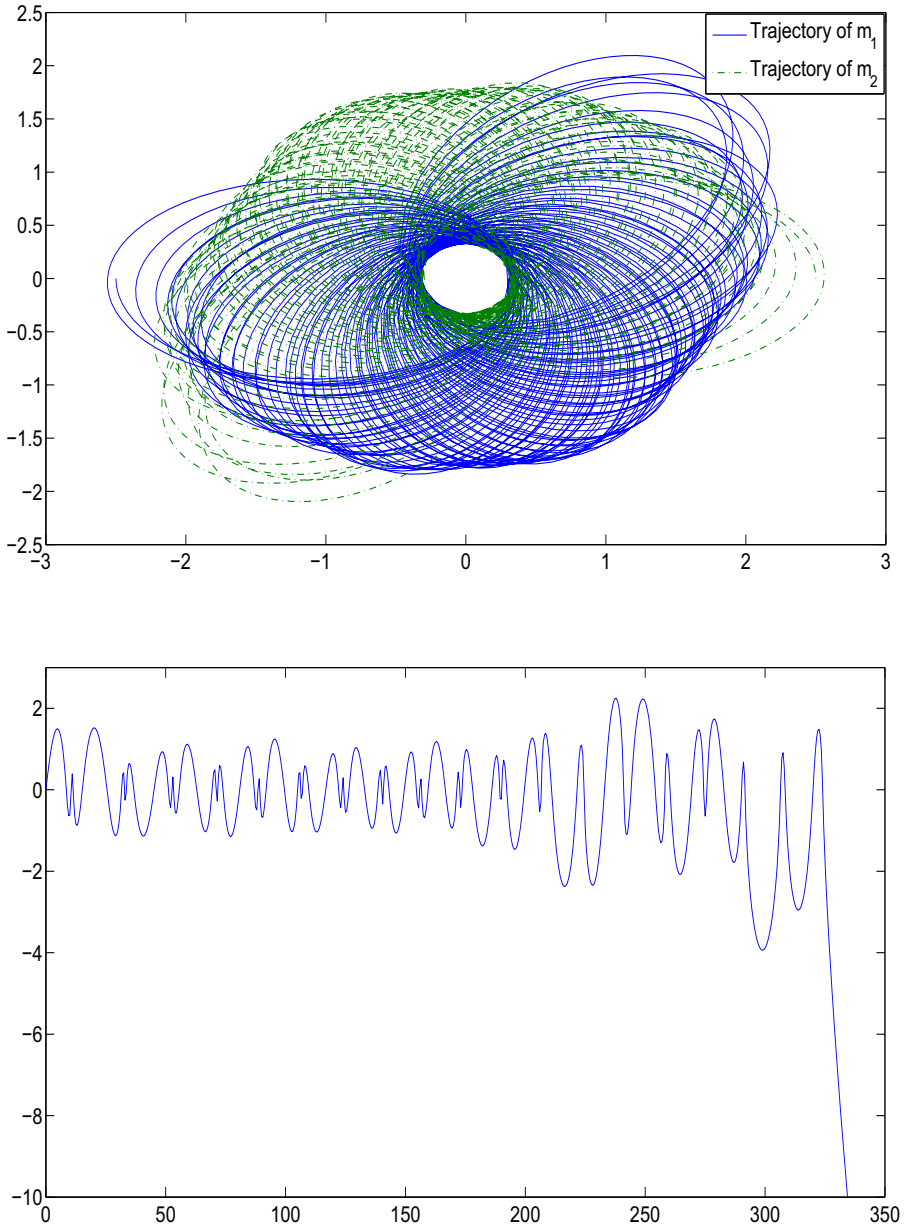

Figure 2.12: The Sitnikov problem solved by the Gauss method of order 4, with stepsize $h = 0.5$, in the time interval $[0, 1500]$. The trajectories of the primaries in the xy-plane (upper picture) exhibit a very irregular behavior which causes the planetoid to eventually escape the system, as illustrated by the space-time diagram in the down picture.

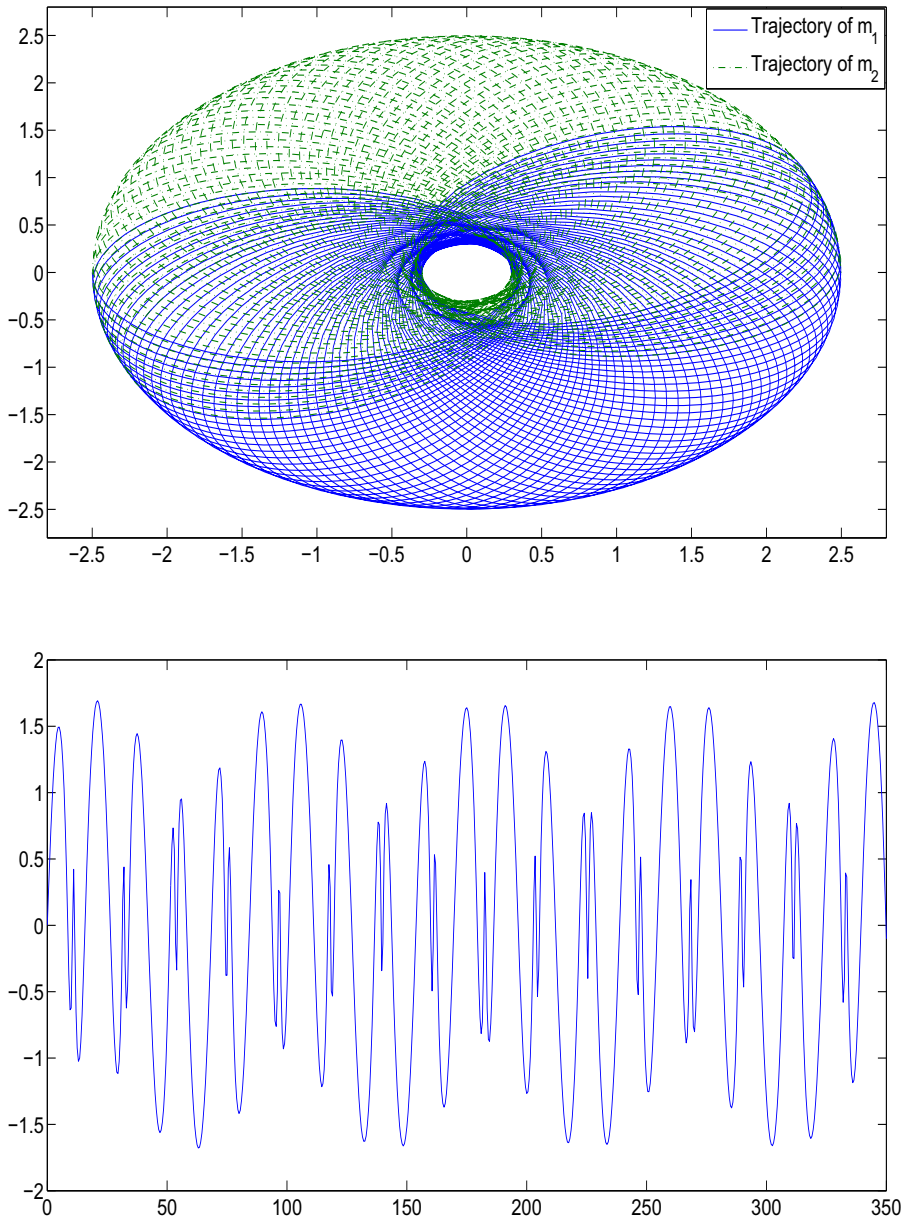

Figure 2.13: The Sitnikov problem solved by the HBVM(18,2) method (order 4), with stepsize $h = 0.5$, in the time interval $[0, 1500]$. Upper picture: the trajectories of the primaries are ellipse shape. The discretization introduces a fictitious uniform rotation of the xy-plane which however does not alter the global symmetry of the system. Down picture: the space-time diagram of the planetoid on the z-axis displayed (for clearness) on the time interval $[0, 350]$ shows that, although a large value of the stepsize h has been used, the overall behavior of the dynamics is well reproduced (compare with the down picture in Figure 2.10).

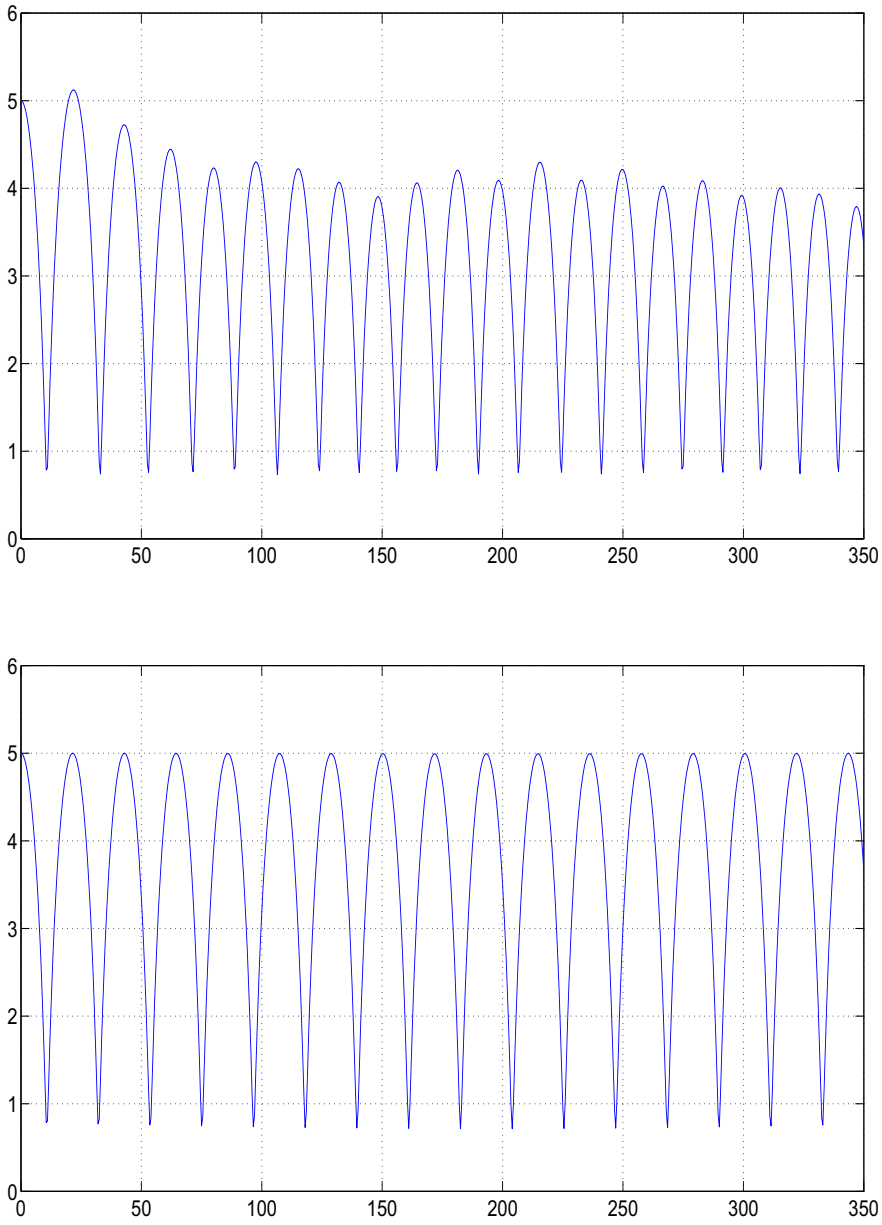

Figure 2.14: Distance between the two primaries as a function of the time, related to the numerical solutions generated by the Gauss method (upper picture) and HBVM(18,2) (down picture). The maxima correspond to the distance of apocentres. These are conserved by HBVM(18,2) while the Gauss method introduces patchy oscillations that destroy the overall symmetry of the system.